Hierarchical structure in Al-Cu alloys to promote strength/ductility synergy

S. H. Wu [a,b], H. Xue [b], C. Yang [b], J. Kuang [b], P. Zhang [b], J.Y. Zhang [b], Y.J. Li [a], Hans J. Roven [a,*], G. Liu [b,*], J. Sun [b,*]

[a]*Department of Materials Science and Engineering, Norwegian University of Science and Technology, 7491 Trondheim, Norway*

[b]*State Key Laboratory for Mechanical Behavior of Materials, Xi'an Jiaotong University, Xi'an, 710049, P.R. China*

Abstract: Experimental evidence demonstrated that equal channel angular pressing (ECAP) at cryogenic temperature, in comparison with ECAP at room temperature, led to promoted strength-ductility synergy in an Al-2.5wt.%Cu alloy. The simultaneous improvement is related to microstructural hierarchy of multimodal grains, low angle grain boundaries, and inter/intragranular precipitates, which was tuned by aging treatment in match with the low-temperature ECAP. The artificial aging could maintain multimodal grain size distribution, introduce a large number of low angle grain boundaries and produce intragranular precipitates to improve strength/ductility. A minor 0.3wt.% Sc addition was effective in optimizing the precipitations and further boosting the strength/ductility combination. The underlying mechanisms for higher strength and greater ductility were rationalized in terms of the low-temperature ECAP.

Key words: Al-Cu alloy; Ultrafine-grained; Microalloying effect; Mechanical properties; Hierarchical microstructure

* Corresponding author: hans.j.roven@ntnu.no (H.J. Roven); lgsammer@mail.xjtu.edu.cn (GL); junsun@mail.xjtu.edu.cn (JS)

With super-high strength, bulk nanostructured (NS) metallic materials have attracted intensive research interests during the past two decades [1-4]. Most researches have been focused on improving the strength and ductility simultaneously [5-11]. The adopted methods include: (i) forming a bimodal/multimodal grain size distribution [7, 9, 10, 12], (ii) generating a high density of intragranular precipitates [5, 6, 8, 13], (iii) introducing a large fraction of nano-twins [11], etc. Recent studies report that severe plastic deformation (SPD) at cryogenic temperature exhibits the ability to improve both strength and ductility, which originates from the suppressed dynamic recovery and dynamic precipitation during SPD deformation [14-18]. Besides, the microalloying effects have also been proven to ameliorate the poor ductility in NS aluminum (Al) alloys and enhance the strength [5, 19]. Thus, designing novel material microstructures by innovative processing routes to improve the mechanical properties of NS materials is still a relentless pursuit in the Al community [1, 20, 21].

Introducing heterogeneous microstructure (*e.g.*, bimodal/multimodal grain structure and heterogeneous lamella structure) in Al alloys can induce an excessively large number of geometrically necessary dislocations (GNDs) to accommodate the large strain gradient during tensile deformation, leading to extra strain hardening and thus better ductility [10, 12, 20, 22, 23]. The precipitation behaviors of SPD processed age-hardening Al alloys have attracted much attention during the past two decades [4, 5, 24-27]. Recent studies reveal that the length-scale dependent Sc microalloying effects in Al-Cu alloys can alter the deleterious intergranular precipitation to favorable intragranular precipitation at the fine/ultrafine-grained length-scale [5, 19], improving the strength and ductility simultaneously. Thus, a coupling of a bimodal/multimodal grain structure and a high density of intragranular precipitates seems to be a promising method to fabricate NS materials with high strength and superior ductility, for which, to the best of the author's knowledge, has received little attention. Besides the aging hardening precipitates, the post-SPD aging can also induce other drastic changes of the microstructure, such as the annihilation of defects (*e.g.*, dislocations and vacancies) at grain boundaries [5, 28, 29], forming a large fraction of low angle grain boundaries (LAGBs) in original micron-sized grains due to the dislocation recovery [10, 28, 30], which can also largely influence the strength [31]. In

present work, the coupling influence of ECAP processing at cryogenic temperature and minor Sc addition on the strength and ductility of Al-Cu alloys is systematically investigated, aiming at offering a new method to fabricate NS Al alloys with superior mechanical properties. A novel hierarchical microstructure is proposed herein to improve the mechanical properties of NS alloys.

Two kinds of alloys with the compositions of Al-2.5wt.%Cu and Al-2.5wt.%Cu-0.3wt.%Sc were respectively cast by using 99.99 wt.% pure Al, 99.99 wt.% pure Cu and Al-2.0wt.% Sc master alloys. All cast ingots were homogenized at 723K for 5h. Bars with dimensions of 100 mm $\times$19.5 mm$\times$19.5mm were machined from the cast ingots for ECAP. After being solution-treated at 873K for 3h and quenched in cold water, the bars were subjected to 4 passes ECAP at both room temperature and cryogenic temperatures by route Bc [32]. For cryogenic ECAP (abbreviated as Cryo-ECAP), the die was kept at 243K in a freezer for 8h before ECAP and was surrounded by dry ice during ECAP to maintain the targeting temperature. All samples were kept in liquid nitrogen for 30 min before and between each ECAP pass. Samples were cut from the uniformly deformed region in the plane containing the normal direction and the extrusion direction (*i.e.*, ND-ED plane) of the ECAP specimens for subsequent microstructure observation and mechanical tests. After ECAP processing, the samples were immediately aged at 398K. Microstructural analyses were carried out using X-ray diffraction (XRD), scanning electron microscopy/electron backscattered diffraction (SEM/EBSD), and high-resolution transmission electron microscopy (HRTEM). The dislocation density was calculated based on the XRD patterns using the Williamson–Hall method [33, 34]. The preparation of SEM-EBSD and TEM specimens were previously reported in [35]. The size and number density of precipitates were measured following the method in [36, 37]. The dog-bone shaped tensile specimens were machined with a gauge size of ~1mm in thickness, 2 mm in width and 6mm in length. Tensile tests were performed at room temperature under a strain rate of 5×10^{-4} s^{-1}, using a laser extensometer.

The evolution of hardness with time during artificial aging at 125°C for Cryo-ECAP Al-2.5Cu and Al-2.5Cu-0.3Sc is shown in Fig. 1 (a). The as-deformed hardness of Cryo-ECAP Al-2.5Cu-0.3Sc is slightly higher than that of Al-2.5Cu, which arises from Al_3Sc particles introduced by solid solution [38, 39] inhibiting dynamic recovery during SPD deformation [40]. Both alloys

exhibit the reducing hardness first until aging to 5h and increasing trend afterwards until the peak aging time. The initial reduction in hardness can be ascribed to the recovery [28], which will be discussed in detail later. The increasing hardness is due to the precipitation of intragranular metastable θ' phase [5, 35]. The peak-aged hardness is significantly higher in Cryo-ECAP Al-2.5Cu-0.3Sc than in Cryo-ECAP Al-2.5Cu.

Engineering stress-strain curves of as-deformed room temperature ECAP (abbreviated as RT-ECAP) [5] and Cryo-ECAP Al-2.5Cu and Al-2.5Cu-0.3Sc alloys are shown in Fig. 1 (b). As-deformed Cryo-ECAP samples present much higher strength and better uniform ductility than as-deformed RT-ECAP ones. Tensile stress-strain curves of peak-aged RT-ECAP [5] and Cryo-ECAP Al-2.5Cu and Al-2.5Cu-0.3Sc alloys are presented in Fig. 1(c). The peak-aged RT-ECAP Al-2.5Cu-0.3Sc presents higher yield strength σ_y (~ 337 MPa vs 280 MPa) and superior ductility (total elongation ~7.5% vs 6% and uniform elongation ~1.3% vs 1%) comparing with the Sc-free counterpart, mainly due to the alteration from partially intergranular precipitation to total intragranular precipitation [5, 35]. Interestingly, the peak-aged Cryo-ECAP Al-2.5Cu-0.3Sc exhibits higher σ_y (~ 380 MPa vs 340 MPa) and better ductility capacity (total elongation ~12% vs 10% and uniform elongation ~4.5% vs 2.3%) than Cryo-ECAP Al-2.5Cu. The improvement in ductility by ECAP at cryogenic temperature, especially uniform elongation, is similar to those achieved by cryogenic ECAP methods in [16, 17]. It's also interesting to note that the ductility of peak-aged Cryo-ECAP Al-2.5Cu is better than that of peak-aged RT-ECAP Al-2.5Cu-0.3Sc, which will be discussed later.

The uniform elongation is mainly determined by the work-hardening rate, $\theta=\partial\sigma / \partial\varepsilon$, where σ is the true stress and ε is the true strain. The Kocks-Mecking plots, *i.e.*, θ-(σ-σ_y) plot, for peak-aged RT-ECAP [5] and Cryo-ECAP Al-2.5Cu and Al-2.5Cu-0.3Sc alloys are shown in Fig. 1(d). The initial work-hardening rate θ_{max} of peak-aged RT-ECAP Al-2.5Cu is the lowest, arising from the smallest dislocation density and number density of intragranular precipitates [27, 41-43]. It can be clearly seen that ECAP at cryogenic temperature can prominently decrease the dynamic recovery rate during tensile deformation (as shown by comparing peak-aged RT-ECAP Al-2.5Cu and Cryo-ECAP Al-2.5Cu), which is more efficient than reported in [16, 17]. Besides, minor Sc

addition can further reduce the dynamic recovery rate during tensile deformation, with peak-aged Cryo-ECAP Al-2.5Cu-0.3Sc presenting the smallest dynamic recovery rate during tensile deformation and thus largest uniform elongation.

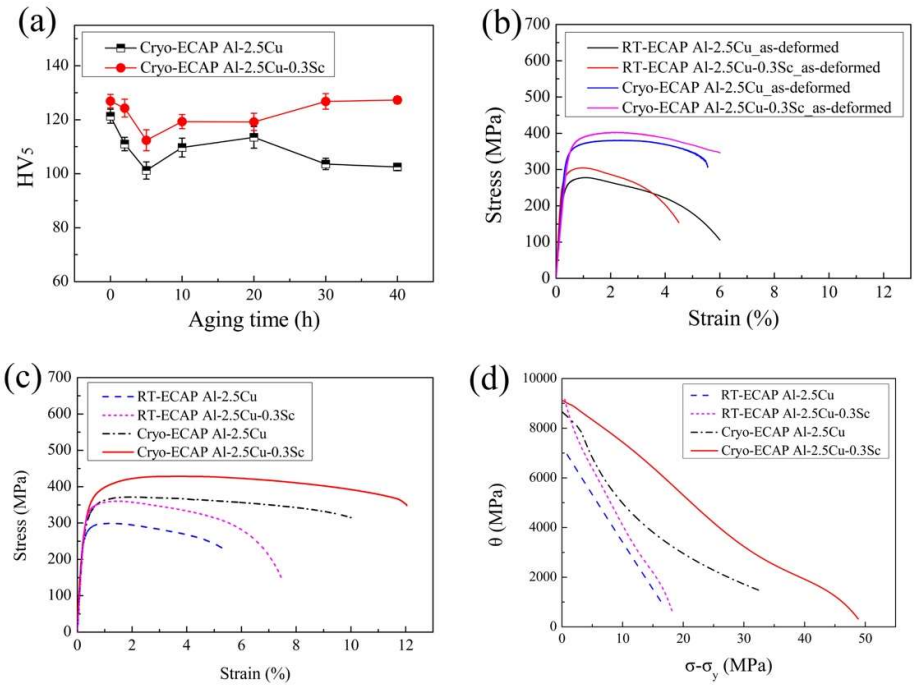

Fig. 1. (a) The evolution of hardness with aging time at 125°C for Cryo-ECAP Al-2.5Cu and Al-2.5Cu-0.3Sc. Engineering stress-strain curves for as-deformed RT-ECAP [5] and Cryo-ECAP Al-2.5Cu and Al-2.5Cu-0.3Sc alloys (b) and for peak-aged RT-ECAP [5] and Cryo-ECAP Al-2.5Cu and Al-2.5Cu-0.3Sc alloys (c). Kocks-Mecking plot for peak-aged RT-ECAP and Cryo-ECAP Al-2.5Cu and Al-2.5Cu-0.3Sc alloys (d).

EBSD images of as-deformed Cryo-ECAP Al-2.5Cu and Al-2.5Cu-0.3Sc are shown in Fig. 2 (a) and (d), respectively. The statistical results of grain size in Fig. 2 (b) and (e) in conjunction with EBSD images clearly show that there exists a multimodal distribution of grain size in both alloys. ECAP at cryogenic temperature leading to the multimodal distribution of grain size can be rationalized in terms of the influence of temperature on activating the dislocation slip system [44, 45]. For those grains possessing less active dislocation slip systems under cryogenic temperature, the grain subdivision by formation of sub-grain boundaries is difficult. Thus, the coarse grains can only be refined to a limited extent. For the other grains with favorable orientations, further ECAP passes can reduce the grain size down to ultrafine/nano range. Furthermore, it's interesting

to note that the multimodal grain size distribution is more prominent with minor Sc addition. This interesting phenomenon can be ascribed to the heterogeneous distribution of fine Al_3Sc particles during SPD deformation, during which the Al_3Sc dispersoids introduced by solid solution [38, 39] can be fragmented into smaller Al_3Sc particles and distribute heterogeneously, *i.e.*, with those grains of favorable orientations distributed with more Al_3Sc particles and the remaining grains depleted of Al_3Sc particles [40, 46]. The smaller Al_3Sc particles can inhibit the motion of dislocations during ECAP, rendering the formation of sub-grain boundaries more difficult. Thus, a more prominent multimodal grain structure can be formed. In Cryo-ECAP Al-2.5Cu, the average misorientation gradient for micron-sized grains lies within 2.1 – 3.0 degree/μm. Meanwhile, in Cryo-ECAP Al-2.5Cu-0.3Sc, the average misorientation gradient for micron-sized grains is within 3.0 – 4.5 degree/μm. This indicates that a higher geometrically necessary dislocation (GND) density exists in the latter alloy [47], which can be roughly estimated by $\rho_{dis} = \theta / b\delta$ (θ is the accumulated misorientation angle in radians within a distance δ, b is the Burgers vector). For example, the misorientation profiles of line L1 and L2 in Fig. 2 (c) and (f) show that a larger misorientation gradient exists in the latter.

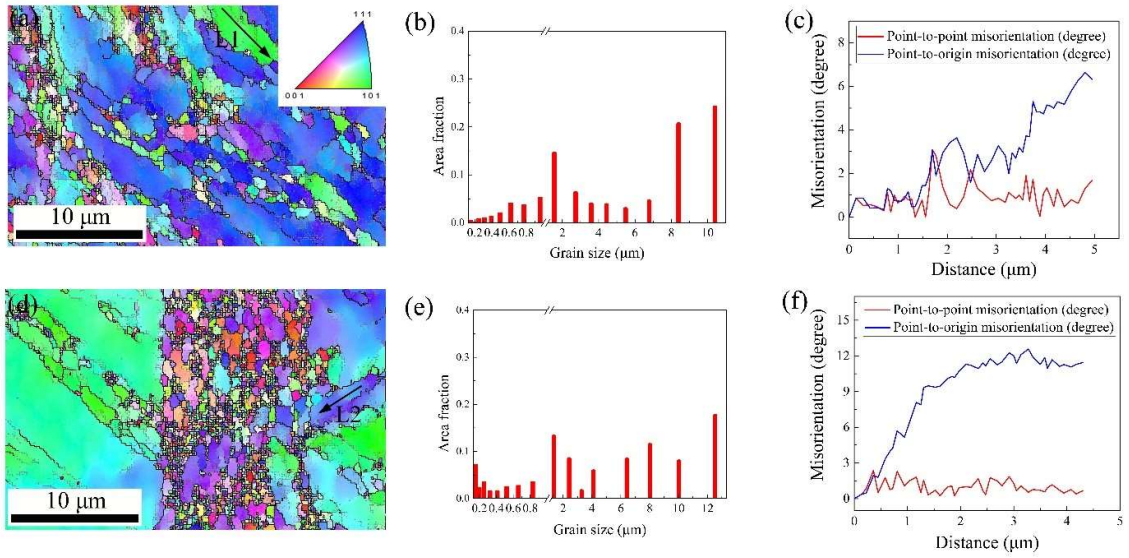

Fig. 2. Typical EBSD images of as-deformed Cryo-ECAP Al-2.5Cu (a) and Al-2.5Cu-0.3Sc (d). (b) and (e) are the corresponding grain size distributions for Al-2.5Cu and Al-2.5Cu-0.3Sc, respectively. (c) and (f) are the

misorientation profiles measured along line L1 and line L2. The narrow grey and coarse black lines depict boundaries with misorientation angles of $2° \le \theta < 10°$ and $\theta \ge 10°$, respectively.

Besides the precipitates, the post-SPD aging can also introduce a large number of LAGBs due to recovery [28], which can also contribute to the strength [30, 48]. The microstructure evolutions of Cryo-ECAP Al-2.5Cu and Al-2.5Cu-0.3Sc aged at 125°C are illustrated by the EBSD images in Fig. 3. A large density of LAGBs with misorientation angles of 6-14° are formed within the coarse micron-sized grains, however, the multimodal grain size distribution is still maintained. Due to the heterogeneous microstructure in the present alloys, we will attempt to describe quantitatively the grain boundary strengthening effect based on the influences of two types of boundaries, *i.e.*, LAGBs and high angle grain boundaries (HAGBs), which can be quantitatively given as the following equation [10, 30]:

$$\sigma_{GB} = \sigma_{HAGB} + \sigma_{LAGB}$$

$$= k_y \left(d_{HAGB}\right)^{-\frac{1}{2}} + M\alpha_1 G\left(1.5bS_V\theta_{ave}^{LAGB}\left(1-f_{HAGB}\right)\right)^{\frac{1}{2}} \quad (1)$$

Where k_y=100 MPa·μm$^{1/2}$ is the Hall-Petch constant for the Al-Cu alloys [15], $\alpha_1 = 0.24$ is a constant depending on the arrangement of dislocations, G=27 GPa is the shear modulus, b=0.286 nm is the Burgers vector for Al, M=3 is the Taylor factor. S_v is the total area of grain boundaries per unit volume, which can be estimated as $S_V = \frac{4}{\pi} B_A$ (B_A is the total boundary length per unit area). θ_{ave}^{LAGB} is the average misorientation angle of LAGBs, f_{HAGB} is the fraction of HAGBs and d_{HAGB} is the size of grains bounded by HAGBs. A cut-off misorientation angle of 10° was chosen [47, 49], since a cut-off angle of 5°/15° can underestimate/overestimate the grain boundary strengthening. The structural parameters derived from the EBSD analysis and calculated grain boundary strengthening for as-deformed, peak-aged alloys are presented in Table 1. The peak-aged grain boundary strengthening reduces somewhat little, arising from that recovery can introduce or sharpen LAGBs. Thus, these boundaries can be correctly identified by EBSD and contribute to the strength.

The precipitate parameters and dislocation density for as-deformed and peak-aged Cryo-ECAP Al-2.5Cu, Al-2.5Cu-0.3Sc alloys are presented in Table 2. The strengthening mechanisms

in present Al-2.5Cu and Al-2.5Cu-0.3Sc alloys processed by ECAP mainly include grain boundary strengthening (σ_{GB}), dislocation strengthening (σ_d) [47], solid solution strengthening (σ_{ss}) [50] and intragranular θ' precipitation strengthening (σ_{Intra}) [5, 38]. The yield strength (σ_y) can be described as [5, 47]:

$$\sigma_y = \sigma_{GB} + \sigma_d + \sigma_{ss} + \sigma_{Intra} \qquad (2)$$

The σ_{GB}, σ_d, σ_{ss}, σ_{Intra}, predicted yield strength σ_y^P using Eq. (2) and experimentally measured yield strength σ_y^E for Cryo-ECAP Al-2.5Cu and Al-2.5Cu-0.3Sc alloys are shown in Table 3. It can be clearly seen that σ_y^P can match well with σ_y^E.

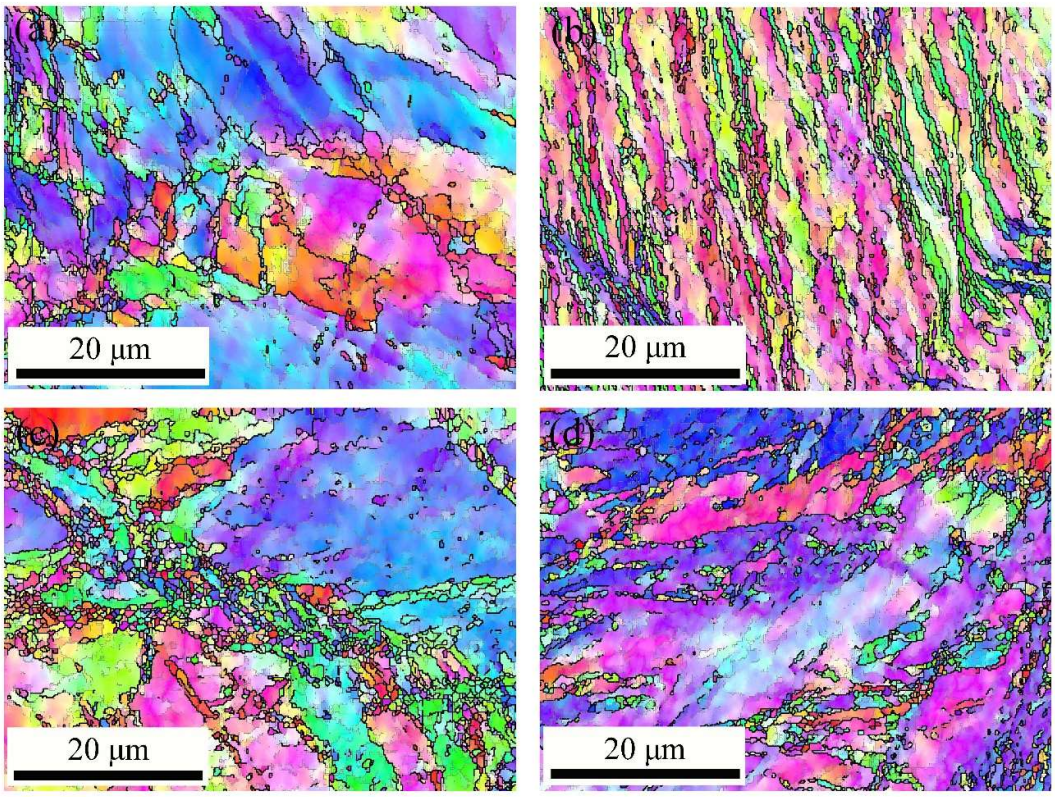

Fig. 3. Typical EBSD images of Cryo-ECAP Al-2.5Cu aged at 125°C for 5h (a) and 20h (b), Cryo-ECAP Al-2.5Cu-0.3Sc aged at 125°C for 5h (c) and 30h (d). The narrow grey and coarse black lines depict boundaries with misorientation angles of $2° \leq \theta < 10°$ and $\theta \geq 10°$, respectively.

Table 1

Structural parameters estimated from the EBSD images and calculated grain boundary strengthening.

	Cut-off angle (°)	θ_{ave}^{LAGB} (°)	f_{HAGB}	S_V (10^6 m^{-1})	d_{HAGB} (μm)	σ_{GB} (MPa)
As-deformed Cryo-ECAP Al-2.5Cu	10	3	0.53	2.8	5.5	148
As-deformed Cryo-ECAP Al-2.5Cu-0.3Sc	10	2.8	0.56	3.2	6.1	145
Peak-aged Cryo-ECAP Al-2.5Cu	10	2.4	0.46	3.8	30	135
Peak-aged Cryo-ECAP Al-2.5Cu-0.3Sc	10	2.3	0.45	4.0	20	140

Table 2

Measurements on the precipitate volume fraction f_{inter} of intergranular precipitates and f_{intra} of intragranular precipitates, mean radius r_{inter} and r_{intra}, number density N_{inter} and N_{intra}, dislocation density in as-deformed, peak-aged Cryo-ECAP Al-2.5Cu and Al-2.5Cu-0.3Sc alloys.

Alloys	**Precipitate parameters**						
	f_{inter}(%)	r_{inter}(nm)	N_{inter} (10^{19}m $^{-3}$)	f_{intra}(%)	r_{intra}(nm)	N_{intra} ($10^{21}$$m^{-3}$)	Dislocation density ($10^{14}$$m^{-2}$)
As-deformed Cryo-ECAP Al-2.5Cu	-	-	-	-	-	-	7.24±1.10
As-deformed Cryo-ECAP Al-2.5Cu-0.3Sc	-	-	-	-	-	-	9.44±1.26
Peak-aged Cryo-ECAP Al-2.5Cu	0.28±0.10	36.6±5.6	1.4±2.5	0.86±0.006	18.5±3.0	1.32±0.22	3.20±0.26
Peak-aged Cryo-ECAP Al-2.5Cu-0.3Sc				2.08±0.18	22.3±1.9	2.03±0.20	3.50±0.40

Table 3

Strengthening effects contribution to the yield strength σ_y for Al-2.5Cu and Al-2.5Cu-0.3Sc alloys.

Alloys	Strengthening effects contribution to the yield strength σ_y (MPa)					
	σ_{GB}	σ_d	σ_{ss}	σ_{Intra}	σ_y^P	σ_y^E
As-deformed Cryo-ECAP Al-2.5Cu	148	147±10	85±8		380±18	363±9
As-deformed Cryo-ECAP Al-2.5Cu-0.3Sc	145	168±11	85±8		398±19	381±7
Peak-aged Cryo-ECAP Al-2.5Cu	135	99±10	40±4	86±8	360±22	340±10
Peak-aged Cryo-ECAP Al-2.5Cu-0.3Sc	140	104±12	30±3	140±10	413±25	390±11

Hierarchical microstructures combining grain size gradient and length-scale dependent precipitation behaviors have been achieved in peak-aged Cryo-ECAP Al-2.5Cu and Al-2.5Cu-0.3Sc alloys, as clearly illustrated in Fig. 4. As shown in Fig. 4 (a), the evolutions of number density of intragranular θ' precipitates with grain size are quite different in both alloys: (i) Al-2.5Cu-0.3Sc presents almost twice higher number density than Al-2.5Cu at the same grain size; (ii) Al-2.5Cu exhibits only intergranular precipitation in grains smaller than ~ 200 nm and intragranular small precipitates/GP zones with grain size lying between 200 nm and 400 nm, above which only intragranular θ' precipitates can be observed; (iii) in contrast Al-2.5Cu-0.3Sc exhibits only intragranular small precipitates/GP zones (as marked by the arrow in Fig. 4 (g)) with grain size lying between ~ 100 nm and ~ 250nm, above which a high number density of intragranular θ' precipitates are formed. This interesting length-scale dependent precipitation behavior in combination with the multimodal grain size distribution can lead to prominent hierarchical microstructures in both alloys, as illustrated in Fig. 4 (b) and (c). It should be noted that a more prominent gradient variation of dislocations can be formed with minor Sc addition, for which the dislocations include GNDs and incidental dislocations [22, 51].

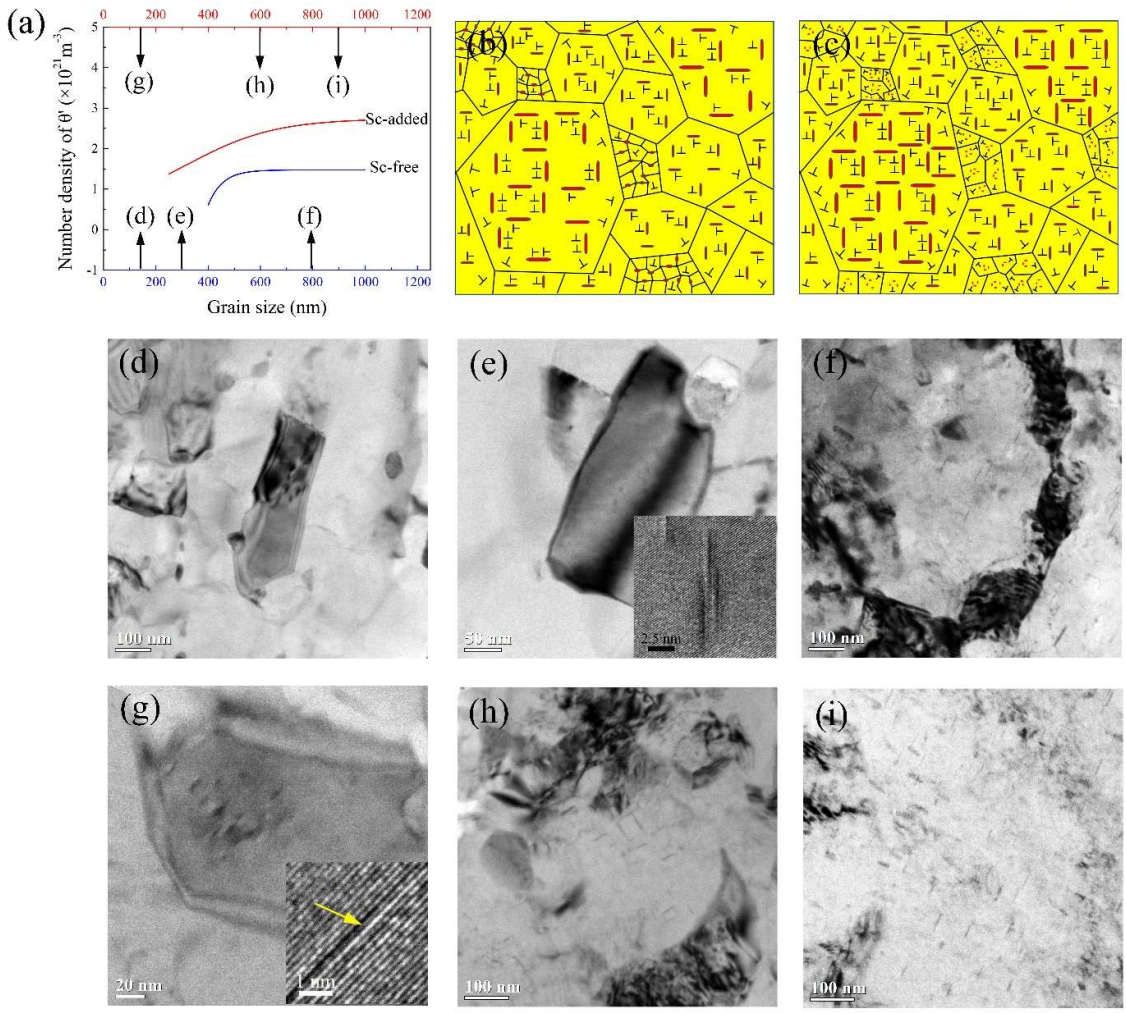

Fig. 4. The evolutions of number density of intragranular θ' precipitate with grain size in peak-aged Cryo-ECAP Al-2.5Cu and Al-2.5Cu-0.3Sc (a) with corresponding bright-field TEM images and magnified images showing the precipitate in (d)-(i). The schematic illustrations of hierarchical microstructures combining length-scale dependent precipitation behaviors, multimodal grain size distribution and a gradient variation of dislocations in peak-aged Cryo-ECAPAl-2.5Cu (b) and Al-2.5Cu-0.3Sc (c).

ECAP processing at cryogenic temperature can lead to higher strength, as quantitatively exhibited in Table 1. It's clearly seen that the enhanced strengthening arises from the improved grain boundary strengthening and dislocation strengthening. The improved grain boundary strengthening can be ascribed to the introduced multimodal grain size distribution, for which a large fraction of LAGBs can significantly contribute to the strength [10, 30, 31]. The enhanced

dislocation strengthening can be due to the suppressed dynamic recovery during ECAP deformation [14, 15].

The significantly improved ductility in peak-aged Cryo-ECAP alloys, as compared with that in peak-aged RT-ECAP alloys, mainly arises from the multimodal grain size distribution and the length-scale dependent θ' precipitates. On one hand, the multimodal grain size distribution leads to gradients of plastic deformation over a length scale of several micrometers during tensile deformation [20, 22]. GNDs will build up to accommodate the deformation incompatibility near grain boundaries between the soft and hard grains [20, 22, 52]. On the other hand, local complex 3D stress states can be induced by the presence of plastic strain gradients during tensile deformation, which will promote the activation of new slip systems and accumulation of incidental dislocations [22, 51]. Thus, the strain gradient introduced GNDs and incidental dislocations can increase the total dislocation density during tensile deformation, leading to enhanced dislocation hardening [20, 22, 51]. The Sc microalloying effect on the length-scale dependent θ' precipitates is prominent, leading to higher density of intragranular θ' precipitates (seen in Fig. 4). The higher density of intragranular θ' precipitates can more efficiently generate, pin down, and thus accumulate dislocations within the grains [5, 6, 8] during tensile deformation, leading to enhanced dislocation/strain hardening [5] .Thus, the coupling of more remarkable multimodal grain size distribution and Sc microalloying effect results in the superior mechanical properties ($\sigma_y \sim 380$ MPa, uniform elongation ~4.5%, and total elongation ~12%) in peak-aged Cryo-ECAP Al-2.5Cu-0.3Sc.

It's interesting to note that peak-aged Cryo-ECAP Al-2.5Cu is more ductile than peak-aged RT-ECAP Al-2.5Cu-0.3Sc, as seen in Fig. 1 (c), even intergranular θ precipitates only exist in the former [5, 35], which are prone to result in intergranular fracture and unresolved low ductility [8, 19]. This interesting phenomenon can be rationalized as follows. In peak-aged Cryo-ECAP Al-2.5Cu, there exists a critical grain size below which intergranular precipitates can be formed. The larger (soft) grains carry much of the plastic strain, and the smaller (hard) grains are difficult to deform [22]. Thus, the detrimental effects of intergranular particles on the ductility can be intelligently minimized. Considering that peak-aged RT-ECAP Al-2.5Cu-0.3Sc possesses higher

density of intragranular θ' precipitates than peak-aged Cryo-ECAP Al-2.5Cu (see Fig. 4 (a) and refer to [5]), it seems that introducing multimodal grain size distribution is more beneficial than enhancing the intragranular precipitates in improving the ductility herein.

In summary, novel hierarchical microstructures combining multimodal grain size distribution and length-scale dependent precipitation can be achieved in peak-aged Cryo-ECAP Al-Cu alloys. Minor Sc addition can further enhance multimodal grain size distribution to increase the total dislocation density and promote intragranular θ' precipitates to strengthen the dislocation storage capacity during tensile deformation. The higher strength in Cryo-ECAP alloys originates from the introduced multimodal grain size distribution. The superior ductility results from the enhanced dislocation/strain hardening during tensile deformation.

Acknowledgements

This work was supported by the National Natural Science Foundation of China (Grant Nos. 51625103, 51722104, 51790482, 51761135031, 52001249 and 52071253), and the 111 Project of China (BP2018008). This work is also supported by the International Joint Laboratory for Micro/Nano Manufacturing and Measurement Technologies. We thank Prof. R.H. Wang at XAUT, Prof. R.H. Zhu, Prof. S.W. Guo, Prof. Y.H. Li and Dr. J. Li at XJTU for their great assistance with TEM analysis. The authors would also thank Mr. Pål C. Skaret for his assistance during ECAP experiments and tensile testing. S.H. Wu thanks for the financial support from the China Scholarship Council (CSC, 201906280171).

References

[1] I.A. Ovid'Ko, R.Z. Valiev, Y.T. Zhu, Prog. Mater. Sci. 94 (2018) 462-540.

[2] X. Sauvage, G. Wilde, S.V. Divinski, Z. Horita, R.Z. Valiev, Mater. Sci. Eng. A 540 (2012) 1-12.

[3] Y. Estrin, A. Vinogradov, Acta Mater. 61 (2013) 782-817.

[4] S.Y. Jiang, R.H. Wang, J. Mater. Sci. Technol. 35 (2019) 1354–1363.

[5] L. Jiang, J.K. Li, G. Liu, R.H. Wang, B.A. Chen, J.Y. Zhang, J. Sun, M.X. Yang, G. Yang, J. Yang, X.Z. Cao, Mater. Sci. Eng. A 637 (2015) 139–154.

[6] S. Cheng, E. Ma, Adv. Mater. 18 (2010) 2280-2283.

[7] Y.M. Wang, E. Ma, Acta Mater. 52 (2004) 1699-1709.

[8] G. Liu, G.J. Zhang, F. Jiang, X.D. Ding, Y.J. Sun, J. Sun, E. Ma, Nat. Mater. 12 (2013) 344-350.

[9] Y.H. Zhao, T. Topping, J.F. Bingert, J.J. Thornton, A.M. Dangelewicz, Y. Li, W. Liu, Y.T. Zhu, Y.Z. Zhou, E.J. Lavernia, Adv. Mater. 20 (2010) 3028-3033.

[10] M. Zha, Y.J. Li, R.H. Mathiesen, R. Bjørge, H.J. Roven, Scr. Mater. 105 (2015) 22-25.

[11] L. Lu, M.L. Sui, K. Lu, Science 287 (2000) 1463-1466.

[12] Y.M. Wang, M.W. Chen, F.H. Zhou, E. Ma, Nature 419 (2003) 912-915.

[13] S. Jiang, R. Wang, J. Mater. Sci. Technol. 35 (2019) 1354–1363.

[14] W. Xu, X.C. Liu, K. Lu, Acta Mater. 152 (2018) 138-147.

[15] W. Xu, L. X.C., X.Y. Li, K. Lu, Acta Mater. 182 (2020) 207-214.

[16] L.H. Su, G.Y. Deng, V. Luzin, H. Wang, A.K. Tieu, Mater. Sci. Eng. A 780 (2020) 139190.

[17] D.C.C. Magalhães, A.M. Kliauga, M.F. Hupalo, O.M. Cintho, V.L. Sordi, Mater. Sci. Eng. A 768 (2019) 138485.

[18] Y.J. Chen, H.J. Roven, S.S. Gireesh, P.C. Skaret, J. Hjelen, Mater. Lett. 65 (2011) 3472-3475.

[19] L. Jiang, J.K. Li, P.M. Cheng, G. Liu, R.H. Wang, B.A. Chen, J.Y. Zhang, J. Sun, M.X. Yang, G. Yang, Sci.Rep. 4 (2014) 3605.

[20] E. Ma, T. Zhu, Mater. Today 20 (2017) 323-331.

[21] G. Wu, C. Liu, L.G. Sun, Q. Wang, B.A. Sun, B. Han, J.J. Kai, J.H. Luan, C.T. Liu, K. Cao, Y. Lu, L.Z. Cheng, J. Lu, Nat. Commun. 10 (2019) 5099.

[22] X.L. Wu, M.X. Yang, F.P. Yuan, G.L. Wu, Y.T. Zhu, Proc. Natl. Acad. Sci. U.S.A. 112 (2015) 14501-14505.

[23] X.C. Meng, B. Liu, L. Luo, Y. Ding, X.X. Rao, B. Hu, Y. Liu, J. Lu, J. Mater. Sci. Technol. 34 (2018) 85-93.

[24] P.V. Liddicoat, X.Z. Liao, Y.H. Zhao, Y.T. Zhu, M.Y. Murashkin, E.J. Lavernia, R.Z. Valiev, S.P. Ringer, Nat. Commun. 1 (2010) 63.

[25] H.J. Roven, M.P. Liu, J.C. Werenskiold, Mater. Sci. Eng. A 483-484 (2008) 54-58.

[26] X. Sauvage, N. Enikeev, R. Valiev, Y. Nasedkina, M. Murashkin, Acta Mater. 72 (2014) 125-136.

[27] E.F. Prados, V.L. Sordi, M. Ferrante, Acta Mater. 61 (2013) 115–125.

[28] H.L. Jia, R. Bjørge, L.F. Cao, H. Song, K. Marthinsen, Y.J. Li, Acta Mater. 155 (2018) 199-213.

[29] X.X. Huang, N. Hansen, N. Tsuji, Science 312 (2006) 249-251.

[30] X.D. Zhang, N. Hansen, Y.K. Gao, X.X. Huang, Acta Mater. 60 (2012) 5933-5943.

[31] K. Lu, Nature Reviews Materials 1 (2016) 16019.

[32] R.Z. Valiev, R.K. Islamgaliev, I.V. Alexandrov, Prog. Mater. Sci. 45(2) (2000) 103-189.

[33] G.K. Williamson, R.E. Smallman, 1 (1956) 34.

[34] K. Ma, H. Wen, H. Tao, T.D. Topping, J.M. Schoenung, Acta Mater. 62(5) (2014) 141-155.

[35] S.H. Wu, P. Zhang, D. Shao, P.M. Cheng, J. Kuang, K. Wu, J.Y. Zhang, G. Liu, J. Sun, Mater. Sci. Eng. A 721 (2018) 200-214.

[36] Q. Feng, S. Jin, S. Gang, Y. Li, Acta Mater. 157 (2018) 114-125.
[37] S.H. Wu, H. Xue, C. Yang, P.M. Cheng, J. Sun, Mater. Sci. Eng. A 812 (2021) 141150.
[38] C. Yang, P. Zhang, D. Shao, R.H. Wang, L.F. Cao, J.Y. Zhang, G. Liu, B.A. Chen, J. Sun, Acta Mater. 119 (2016) 68-79.
[39] J.Y. Zhang, Y.H. Gao, C. Yang, P. Zhang, J. Kuang, G. Liu, J. Sun, Rare Metals 39 (2020) 636–650.
[40] Y. Buranova, V. Kulitskiy, M. Peterlechner, A. Mogucheva, R. Kaibyshev, S.V. Divinski, G. Wilde, Acta Mater. 124 (2017) 210-224.
[41] U.F. Kocks, H. Mecking, Prog. Mater. Sci. 48 (2003) 171-273.
[42] Y. Estrin, H. Mecking, Acta Metallurgica 32 (1984) 57-70.
[43] K.-W. D, Trans Met Soc AIME 218 (1962) 962.
[44] M. Carrard, J.L. Martin, Philos. Mag. A 56 (1988) 391-405.
[45] D. Caillard, J.L. Martin, Int. J. Mater. Res. 100 (2009) 1403-1410.
[46] B.K. Min, H.W. Kim, S.B. Kang, J. Mater. Proc. Tec. 162 (2005) 355-361.
[47] M. Zha, Y. Li, R.H. Mathiesen, R. Bj?Rge, H.J. Roven, Acta Mater. 84 (2015) 42-54.
[48] T.L. Huang, L.F. Shuai, A. Wakeel, G.L. Wu, N. Hansen, X.X. Huang, Acta Mater. 156 (2018) 369-378.
[49] N. Kamikawa, X. Huang, N. Tsuji, N. Hansen, Acta Mater. 57 (2009) 4198-4208.
[50] F.R.N. Nabarro, Theory of Crystal Dislocations, Oxford University Press, oxford, 1967.
[51] X.L. Wu, P. Jiang, L. Chen, F. Yuan, Y.T. Zhu, Proc. Natl. Acad. Sci. U.S.A. 111 (2014) 7197-7201.
[52] Ashby, F. M., Philos. Mag. 21 (1970) 399-424.